

# Influence of polydispersity on the critical parameters of an effective potential model for asymmetric hard sphere mixtures

Julio Largo<sup>1</sup> and Nigel B. Wilding<sup>1</sup>

<sup>1</sup>*Department of Physics, University of Bath, Bath BA2 7AY, United Kingdom*

(Dated: December 20, 2021)

We report a Monte Carlo simulation study of the properties of highly asymmetric binary hard sphere mixtures. This system is treated within an effective fluid approximation in which the large particles interact through a depletion potential (R. Roth *et al*, Phys. Rev. E **62** 5360 (2000)) designed to capture the effects of a virtual sea of small particles. We generalize this depletion potential to include the effects of explicit size dispersity in the large particles and consider the case in which the particle diameters are distributed according to a Schulz form having degree of polydispersity 14%. The resulting alteration (with respect to the monodisperse limit) of the metastable fluid-fluid critical point parameters is determined for two values of the ratio of the diameters of the small and large particles:  $q \equiv \sigma_s/\sigma_b = 0.1$  and  $q = 0.05$ . We find that inclusion of polydispersity moves the critical point to lower reservoir volume fractions of the small particles and high volume fractions of the large ones. The estimated critical point parameters are found to be in good agreement with those predicted by a generalized corresponding states argument which provides a link to the known critical adhesion parameter of the adhesive hard sphere model. Finite-size scaling estimates of the cluster percolation line in the one phase fluid region indicate that inclusion of polydispersity moves the critical point deeper into the percolating regime. This suggests that phase separation is more likely to be preempted by dynamical arrest in polydisperse systems.

PACS numbers: 64.70Fx, 68.35.Rh

## I. INTRODUCTION AND BACKGROUND

Highly asymmetric mixtures of hard spheres have long served as a prototype model for systems of large colloidal particles dispersed in a sea of smaller colloids. A key physical feature of such systems is the mediation by the small particles of so-called depletion forces between the large ones [1]. This force has its origin in entropic effects associated with the dependence of the free volume of the small particles on the degree of clustering of the large ones. Although, the typical range of the forces is rather limited (of order the diameter of the small particles), they can be very strong.

A longstanding issue in this context concerns the ability of depletion forces to engender phase transitions in binary hard sphere mixtures. Biben and Hansen [2] addressed this matter using integral equation theory, and predicted that for sufficient size asymmetry, depletion forces engender a fluid-fluid spinodal instability. Other theoretical studies have arrived at often conflicting conclusions in this regard (see discussion in ref. [3]), but experiments on colloidal systems (eg. ref. [5]), do apparently confirm a transition, although in certain circumstances it is found to be metastable with respect to a broad fluid-solid coexistence region.

Ideally one would like to settle the matter of the existence of a fluid-fluid transition (as well as its stability or otherwise with respect to the fluid-solid boundary), by computer simulation. Unfortunately, direct simulation studies of very asymmetric additive mixtures are severely hampered by extremely slow relaxation. Accordingly, all such studies to date have been restricted to mixtures of relatively low asymmetries, for which a fluid-fluid transition is less likely to be observable. While recently de-

veloped novel algorithms [6, 7] offer some hope of future progress in accessing greater size asymmetries, no direct evidence has (to date) been obtained for the existence of a fluid-fluid phase separation in additive hard sphere mixtures.

In view of these difficulties, a fruitful alternative to simulations of the full two component mixture is to attempt to map it onto an effective one-component system which can be simulated more easily. This “effective fluid” approach was taken by Dijkstra, van Roij and Evans [3], and by Almaraz and Enciso [4] who proposed a model depletion potential by tracing out from the partition function the degrees of freedom associated with the small particles. The resulting interparticle potential for the large particles is parameterized by the size ratio  $q = \sigma_s/\sigma_b$  between small and large particles, and a *reservoir* volume fraction of the small particles  $\eta_s$ . Simulation-based free energy measurement of the resulting system yielded, for values of  $q < 0.1$ , a fluid-fluid separation that was metastable with respect to a broad solid-fluid coexistence region. Explicit simulations of the two component mixture confirmed the accuracy of the model depletion potential as far as the location of solid-fluid and solid-solid transitions was concerned, but could not access the likely region of fluid-fluid separation. Subsequent work by Roth, Evans and Dietrich [8] yielded a more accurate depletion potential by fitting to accurate DFT predictions. However to our knowledge the latter potential has to date not been used to study phase behaviour.

Real colloidal fluids are polydisperse, that is their constituent particles exhibit an essentially continuous range of size, shape or charge. Introducing polydispersity into model fluids is known to alter fluid-fluid critical point parameters [9, 10] as well as freezing boundaries [11, 12]. It

is therefore pertinent to enquire as to the effect of polydispersity on the location of the metastable fluid-fluid transition of hard sphere mixtures. Indeed this question has previously been addressed in part by Warren [13] who applied the moment free energy method [14] to study a polydisperse version of the equation of state of Boublik and Mansoori [15] for binary hard sphere mixtures. The results showed that for sufficiently large size ratio and polydispersity of the large particles, a fluid-fluid spinodal appears in the model. The transition was predicted to become more stable with increasing degree of polydispersity.

Most other theoretical investigations of polydispersity in hard sphere mixtures [16–18] have focussed on the form of the depletion potential and did not explicitly consider the consequences for phase equilibria. The sole study of phase behaviour to date (of which we are aware) is that of Fasolo and Sollich [11] who applied the moment free energy method to the Asakura-Oosawa (AO) model [19]. This model describes the limit of maximum non-additivity of the small particles and in contrast to additive mixtures, the monodisperse AO model is known to exhibit a *stable* fluid-fluid phase transition for size ratios  $q \lesssim 0.5$  [20, 21]. The introduction of size polydispersity to the large spheres [11] was observed to disfavor both fluid-fluid and fluid-solid phase separation, though the effect was larger for the latter transition. The net result was a lowering of the  $q$  value necessary for occurrence of stable fluid-fluid phase separation, and an increase in the stability of this transition with respect to freezing.

In the present work we apply specialized Monte Carlo simulation techniques to an effective fluid model for additive mixtures with a view to elucidating the effect of large particle (colloidal) polydispersity on the parameters of the fluid-fluid critical point. Our results indicate that polydispersity shifts the critical point to lower reservoir volume fractions  $\tilde{\eta}_s$  of the smaller particles, and to higher volume fractions  $\eta_b$  of the large ones. A determination of the percolation threshold using finite-size scaling methods shows that the addition of polydispersity moves the fluid-fluid critical point deeper into the percolation region. We further find that accurate predictions for the critical reservoir volume fraction  $\tilde{\eta}_s^{\text{crit}}$  can be obtained by matching the second virial coefficient of the depletion potential to that of the adhesive hard sphere model at its (independently known) critical point.

## II. MODELS

### A. Depletion potentials

Two model depletion potentials are considered in this work. The first, on which we shall focus primarily, is due to Roth, Evans and Dietrich [8], and we shall refer to it as the RED potential. It derives from accurate density functional theory (DFT) studies of hard sphere mixtures and takes the form:

$$W = \epsilon \frac{R_b + R_s}{2R_s} \bar{W}. \quad (1)$$

Here  $R_b$  and  $R_s$  are the radii of the large and small spheres respectively. The scaled depletion potential  $\bar{W} = \bar{W}(x, \eta_s)$  is a function of  $x = h/\sigma_s$ , the distance from contact measured in units of the small sphere diameter, and the volume fraction  $\eta_s$  of the small spheres. The parameter  $\epsilon$  takes the value  $\epsilon = 2$  for wall-sphere interactions and  $\epsilon = 1$  for sphere-sphere interactions.

Between contact at  $x = 0$  and the location of the first maximum  $x_0$  the scaled depletion potential is expressed in terms of a cubic polynomial:

$$\beta \bar{W}(x, \eta_s) = a(\eta_s) + b(\eta_s)x + c(\eta_s)x^2 + d(\eta_s)x^3, \quad x \leq x_0. \quad (2)$$

The coefficients  $a, b, c$  and  $d$  were obtained by Roth *et al* by fitting to depletion potentials calculated within DFT. For  $x > x_0$ , they assume that the asymptotic regime already sets in. For the interaction between two spheres (a different expression applies to the asymptotic behaviour between a sphere and a hard wall) this is

$$\beta \bar{W}(x, \eta_s) = \beta \bar{W}^{\text{asym}}(x, \eta_s), \quad x > x_0 \quad (3)$$

where

$$\beta \bar{W}^{\text{asym}}(x, \eta_s) = \frac{A_p(\eta_s)}{\sigma_s^{-1}(\sigma_b + h)} \exp(-a_0(\eta_s)\sigma_s x) \times \cos[a_1(\eta_s)\sigma_s x - \Theta_p(\sigma_s)], \quad x > x_0 \quad (4)$$

Here the denominator measures the separation between the centers of the spheres in units of  $\sigma_s$ , and the prefactors  $a_0(\eta_s)$  and  $a_1(\eta_s)$  can be calculated from the Percus-Yevick bulk pair direct correlation function [8]. The amplitude  $A_p(\eta_s)$  and phase  $\Theta_p(\eta_s)$  are chosen such that the depletion potential and its first derivative are continuous at  $x_0$ . They are weakly dependent on the size ratio. Fig. 1 shows the form of the potential for the size ratio  $q = 0.1$  at a selection of values of  $\eta_s$ .

The RED potential was tested in ref. [8] by comparing with computer simulation results for hard sphere mixtures and was found to perform well for volume fractions of the small particles in the range  $0 < \eta_s < 0.3$ . In the simulations to be described below, we use a truncated version of the RED potential, cutoff at  $x = 0.3$ , and with no correction. Furthermore we shall employ the potential at finite volume fractions  $\eta_b$  of the large particles, but assume the potential remains two-body in form, being parameterised by the reservoir volume fraction of small particles  $\tilde{\eta}_s$ , which plays a role similar to a chemical potential. Clearly  $\tilde{\eta}_s \rightarrow \eta_s$  in the limit  $\eta_b \rightarrow 0$ . We note that approximate expressions exist which allow one to convert from  $\tilde{\eta}_s$  to  $\eta_s$  at finite  $\eta_b$  [3], at least in the monodisperse case.

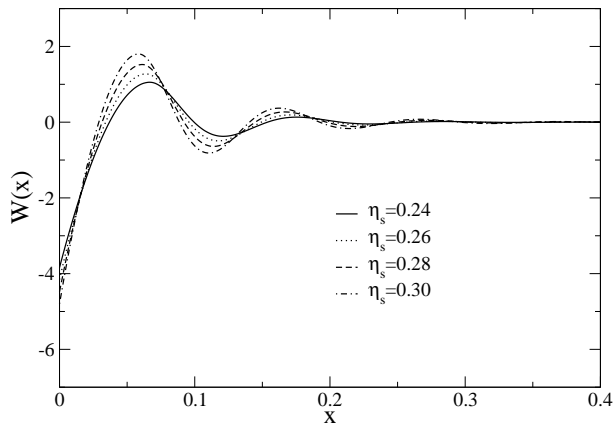


FIG. 1: The form of the RED potential for  $q = 0.1$  at a selection of values of  $\eta_s$ .

The second potential that we have studied, albeit to a lesser extent and solely in the monodisperse context, is that due to Götzelmann et al [22, 23]. In contrast to the DFT-based RED potential, this was derived purely within the framework of the Derjaguin approximation, although it too is expressed as a series expansion. We shall employ it in the truncated form studied by Dijkstra, van Roij and Evans [3], and refer to as the DRE potential:

$$\beta V_{\text{eff}}(r_{ij}) = -\frac{1+q}{2q} [3\lambda^2\tilde{\eta}_s + (9\lambda + 12\lambda^2)\tilde{\eta}_s^2 + (36\lambda + 30\lambda^2)\tilde{\eta}_s^3]; \quad -1 < \lambda < 0 \quad (5)$$

where  $\lambda = x - 1$ .

Although both potentials have a qualitatively similar form at short range, the DRE potential neglects the correct damped oscillatory decay at larger particle separations. A comparison of the two potentials for size ratio  $q = 0.1$  and  $\tilde{\eta}_s = 0.3$  is shown in fig. 2.

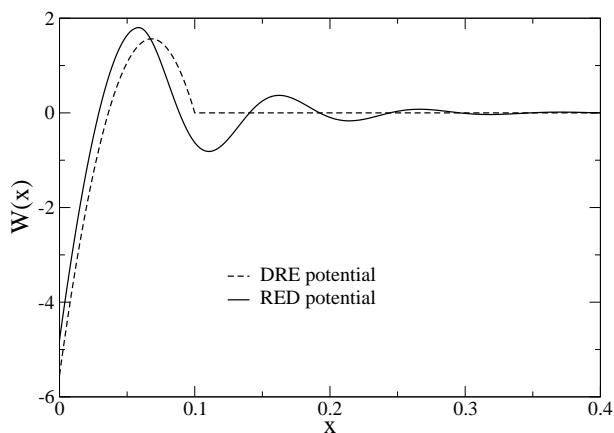


FIG. 2: Comparison of the RED and DRE potentials for  $q = 0.1$  and  $\tilde{\eta}_s = 0.3$ .

## B. Incorporating polydispersity

The key to incorporating polydispersity into the above framework is to generalize the form of the depletion potential for the case of two interacting large particles of *different* radii  $R_1$  and  $R_2$ . This is readily achieved by appeal to the Derjaguin approximation [24, 25], which relates the depletion force between two spheres of different radii ( $R_1$  and  $R_2$ ) to the potential between two flat plates:

$$F_{ss} = 2\pi \frac{R_1 R_2}{R_1 + R_2} U_{ww}(h). \quad (6)$$

The approximation also yields the force between a sphere (of radius  $R$ ) and a wall:

$$F_{sw} = 2\pi R U_{ww}(h) \quad (7)$$

Clearly, if the two spheres in the first case have equal radii ( $R_1 = R_2$ ), then

$$F_{ss} = \pi R U_{ww}(h), \quad (8)$$

giving the well known result  $F_{sw} = 2F_{ss}$ .

Returning to the depletion potential of eq. 1, the above considerations prompt one to write:

$$W = \frac{R'_1 R'_2}{R'_1 + R'_2} \bar{W} \quad (9)$$

where

$$R'_1 = \frac{R_1 + R_s}{R_s} \quad (10)$$

$$R'_2 = \frac{R_2 + R_s}{R_s} \quad (11)$$

It is readily verifiable that in the limiting cases  $R_1 \rightarrow \infty$  and  $R_1 \rightarrow R_2$ , one recovers the expression of Roth et al [8] (eq. 1) with  $\epsilon = 2$  and  $\epsilon = 1$  respectively.

With regard to the effect of this generalization on the parameterized form of the potential, we note firstly that the quantity  $x$  remains unaffected because it is simply the distance from contact in units of  $\sigma_s$ . However, in the asymptotic part (eq. 4), the denominator  $\sigma_s^{-1}(\sigma_b + h)$  measuring the separation between the centers of the spheres in  $\sigma_s$  units is given in the polydisperse case by  $\sigma_s^{-1}[(\sigma_1 + \sigma_2)/2 + h]$ . Additionally, while in the monodisperse limit the location of the first maximum of the potential (at which the asymptotic behaviour is presumed to set in) is given by  $x_0 = \sigma_s^{-1}(\sigma_s + \sigma_b)$ , in the polydisperse case one has instead  $x_0 = \sigma_s^{-1}[\sigma_s + (\sigma_1 + \sigma_2)/2]$ . Fig. 3 gives some examples of the influence of dissimilar particle sizes on the depletion potential.

In the present work, we address the situation in which the large particles exhibit a continuous variation of sizes.

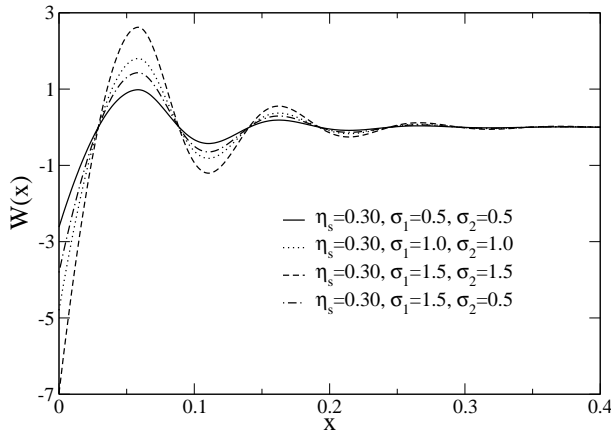


FIG. 3: The form of the RED depletion potential for four combinations of the pair radii. In all cases we have set  $\sigma_s = 0.1$

In order to quantify the form of the polydispersity, we label each particle by the value of its diameter  $\sigma_b$ . The system can then be described in terms of a density distribution  $\rho(\sigma_b)$  measuring the number density of particles of each  $\sigma_b$ . Experimentally, the distribution of colloidal particles sizes in a system is (in general) *fixed* by the synthesis of the fluid. To reflect this situation in our simulations, we assign  $\rho(\sigma_b)$  an ad-hoc prescribed functional form, which we choose to be of the Schulz type [26] defined by the normalized distribution function:

$$f(\sigma_b) = \frac{1}{z!} \left( \frac{z+1}{\bar{\sigma}_b} \right)^{z+1} \sigma_b^z \exp \left[ - \left( \frac{z+1}{\bar{\sigma}_b} \right) \sigma_b \right]. \quad (12)$$

Here  $z$  is a parameter which controls the width of the distribution, while  $\bar{\sigma}_b \equiv 1$  sets the length scale. We have elected to study the case  $z = 50$ , for which the corresponding form of  $f(\sigma_b)$  is shown in fig. 4. The associated degree of polydispersity is defined as the normalized standard deviation of the size distribution:

$$\delta = \frac{\langle (\sigma_b - \bar{\sigma}_b)^2 \rangle^{\frac{1}{2}}}{\bar{\sigma}_b} \quad (13)$$

For the Schulz distribution one finds  $\delta = 1/\sqrt{z+1}$ . With  $z = 50$ , this formula yields  $\delta \approx 14\%$ . Note that for computational convenience, lower and upper cutoffs were imposed on the range of allowed particle sizes  $\sigma_b$ . These were chosen such that  $0.5 \leq \sigma_b \leq 1.5$ .

The imposed density distribution is related to  $f(\sigma_b)$  by

$$\rho(\sigma_b) = \rho_b^0 f(\sigma_b) \quad (14)$$

where  $\rho_b^0$  is the average number density of large particles. Since  $f(\sigma_b)$  is fixed, the form of  $\rho(\sigma_b)$  is parameterized solely by  $\rho_b^0$ , variations of which correspond (at a given  $\tilde{\eta}_s$ ) to traversing a “dilution line” in the full finite

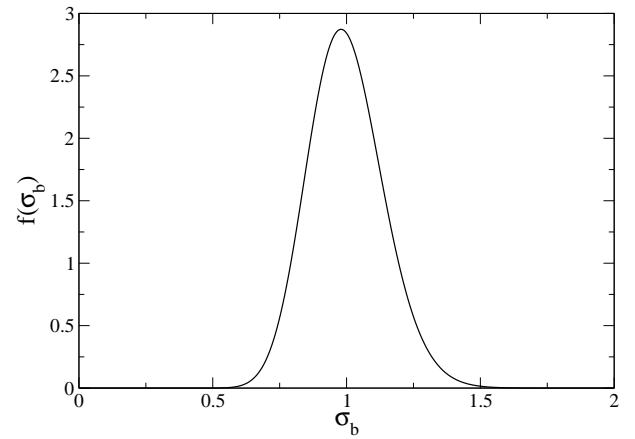


FIG. 4: The imposed form of  $f(\sigma_b)$ , corresponding to a Schulz distribution (eq. 12) with  $z = 50$ . The diameters  $\sigma_b$  of the large particles are measured in units of  $\bar{\sigma}_b = 1$

dimensional phase diagram [27]. Although this parameterization provides the operational basis for scanning the dilution line, we shall (in accordance with convention) quote our results in terms of the overall *volume fraction* of the large particles. The latter is related to the density distribution via

$$\eta_b = \int_0^\infty \frac{\pi}{6} \sigma_b^3 \rho(\sigma_b) d\sigma_b. \quad (15)$$

Finally in this section, we note that within the polydisperse context, the distribution of sizes of the large particles implies that the size ratio  $q$  can only be defined in terms of an average. Accordingly we take  $q \equiv \sigma_s/\bar{\sigma}_b$ .

### III. COMPUTATIONAL METHODS

Monte Carlo simulations were performed within the grand canonical ensemble GCE using the methods described in refs. [10, 28–30]. Here we briefly outline principal elements of the strategy and refer the interested reader to those papers for a fuller description.

Within the GCE framework, the density distribution  $\rho(\sigma_b)$  is obtained as an ensemble average over an instantaneously fluctuating distribution. The form of  $\rho(\sigma_b)$  is controlled by the conjugate chemical potential distribution  $\mu(\sigma_b)$ , which was tuned (cf ref. [30]) at all points in the phase diagram such as to yield the desired Schulz shape  $f(\sigma)$  (eqs. 12, and scale  $\rho_b^0$  14). This tuning was achieved by joint use of the non-equilibrium potential refinement (NEPR) method [29], coupled with histogram extrapolation [31] in terms of  $\mu(\sigma_b)$ . It should be noted, however, that the DRE and RED depletion potentials do not lend themselves to histogram extrapolation with respect to the model parameter  $\tilde{\eta}_s$  which controls the form of the interaction potential. This is because  $\tilde{\eta}_s$  does not appear as an overall scale factor in the Hamiltonian,

a situation which contrasts, for example, to temperature reweighting in simpler potentials such as Lennard-Jonesium. Consequently in order to scan the phase diagram with respect to changes in  $\tilde{\eta}_s$ , separate simulations were utilized in each instance.

Our principal aim is a determination of the polydispersity-induced shifts in the critical point parameters of the model depletion potentials. To this end we have employed a crude version of the finite-size scaling (FSS) analysis described in ref. [32]. The analysis involves scanning the range of  $\rho_b^0$  and  $\tilde{\eta}_s$  until the observed probability distribution of the fluctuating instantaneous volume fraction of large particles  $p(\eta_b)$ , matches the independently known universal fixed point form appropriate to the Ising universality class in the FSS limit. Owing to the relatively large depth of the interparticle potential well (see fig. 2) compared to eg. the Lennard-Jones (LJ) potential, the acceptance rate for particle insertions and deletions was found to be very low, resulting in extended correlation time for the density fluctuations. Consequently we were able neither to study a wide range of system sizes nor obtain data of sufficient statistical quality to permit a more sophisticated FSS analysis. Nevertheless it transpires that our estimated uncertainties on the critical point parameters are sufficient to resolve the polydispersity-induced trends in the critical point parameters that we set out to identify.

#### IV. SIMULATION RESULTS

Our results are divided into three sections. Firstly we locate the fluid-fluid critical point for both the RED and DRE potentials in the monodisperse limit. Moving on to the polydisperse case, we determine the effect of the added polydispersity on the critical point parameters. Finally we use finite-size scaling to estimate the locus of the cluster percolation threshold in both the mono- and poly-disperse cases.

##### A. Monodisperse limit

###### 1. Critical region

As outlined above, we have tuned the values of  $\tilde{\eta}_s$  and  $\mu$  until the measured probability distribution of the volume fractions of the large particles matched (as far as possible given the computational complexity of this problem) the universal Ising fixed point form. Fig. 5 shows distributions obtained in this way for the case of the RED potential with  $q = 0.1$  at  $\tilde{\eta}_s = 0.3200$  and  $\tilde{\eta}_s = 0.3190$ . Although the statistical quality is not particularly good, comparison of the forms of the distributions with that of the fixed point form indicates that the given values of  $\tilde{\eta}_s$  straddle criticality, permitting the estimate  $\tilde{\eta}_s^{\text{crit}} = 0.3195(5)$ . This estimate for the RED potential critical point, together for that for  $q = 0.05$ ,

RED potential		
$q$	$\tilde{\eta}_s^{\text{crit}}$	$\eta_b^{\text{crit}}$
0.1	0.3195(5)	0.274(10)
0.05	0.1765(5)	0.289(15)

DRE potential		
$q$	$\tilde{\eta}_s^{\text{crit}}$	$\eta_b^{\text{crit}}$
0.1	0.255(15)	0.286(15)
	[0.289]	[0.223]
0.05	0.151(1)	0.271(15)
	[0.165]	[0.235]

TABLE I: Estimates of critical point parameters, obtained using the methods described in the text. Values estimated from the data of ref.[3] are given in square brackets.

and the corresponding estimates for the DRE potential are presented in tab. I.

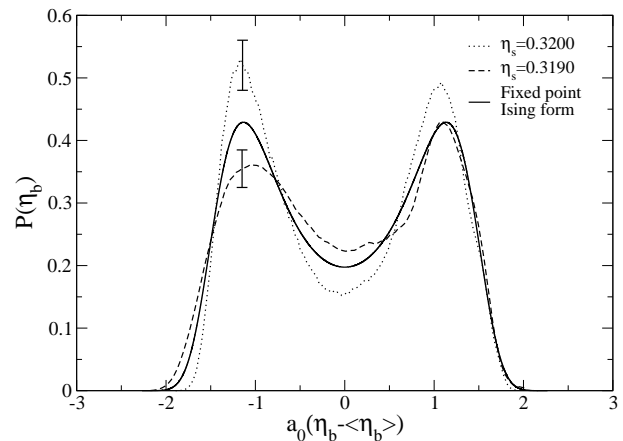


FIG. 5: Estimates of the order parameter distribution  $p(\eta_b)$  at  $\tilde{\eta}_s = 0.3200$  and  $\tilde{\eta}_s = 0.3190$ , for  $V = (5.2\sigma)^3$ . Representative error bars are shown. Also included is the fixed point Ising magnetisation distribution. All distributions are scaled to unit norm and variance via the non-universal scale factor  $a_0$ .

With regard to the results, of tab. I, we note that for a given potential form, the estimates of  $\eta_b^{\text{crit}}$  appear rather insensitive to the value of  $q$ . We further note that for a given  $q$  there is a substantial shift in  $\tilde{\eta}_s^{\text{crit}}$  between the two forms of the depletion potential. The latter finding is perhaps not too surprising given the significant difference in the contact value and range of the well depth of the RED and DRE potentials, as well as the rather radical truncation made by the DRE potential, of the long ranged oscillatory part of the interactions (cf. fig. 2). Indeed the sensitivity of phase behaviour to the depletion potential well depth and range has been emphasised by Germain *et al* [33], albeit in the context of fluid-solid coexistence.

We also note significant discrepancies between our estimates of the critical point and those of Dijkstra *et al*

[3] for the DRE potential. Although no error bars are quoted in ref.[3], it seems likely to us that this discrepancy is statistically significant. Its source may be traceable to the use in [3] of indirect free energy measurements to obtain the phase diagram, in contrast to the generally more accurate direct grand canonical FSS approach employed here. Interestingly, our estimates for the critical  $\tilde{\eta}_s$  values lie much closer than those of ref. [3] to the results of a computation using integral equation theory of both the depletion potential and its phase behaviour [34].

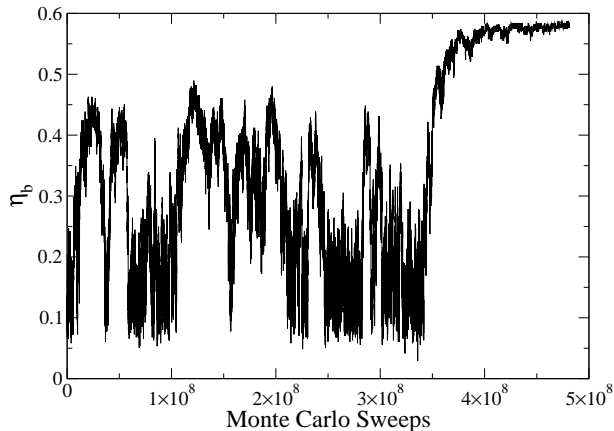


FIG. 6: Time evolution of the system volume fraction near the parameters of the metastable critical point. Eventually, the system freezes spontaneously.

In ref. [3] it was demonstrated via free energy measurements that the fluid-fluid critical point for the DRE potential is metastable with respect to freezing. While we have not attempted to perform a systematic study of the freezing transition in the present work, our simulations confirm the metastability in so far as some runs were observed to freeze into an f.c.c. crystal structure. An example of the time evolution of the density in such a run for the DRE potential is shown in fig. 6. Such freezing was also observed for the RED potential indicating that here too the critical point is metastable with respect to crystallization. As an aside, we note that from a computational point of view, our observation of freezing within the grand canonical ensemble is somewhat remarkable since the algorithm becomes very inefficient at crystal densities. The key factor in achieving this in the present case is the inclusion—alongside the standard insertions, deletions and resizing moves—of particle displacement moves. Without the latter, the system was not observed to crystallize on simulation time scales. Another apparent factor controlling the ease of freezing appears to be whether the crystal lattice parameter is commensurate with the choice of system box size. We further note that our frozen structures do not attain the near-close packing densities observed in ref. [3]. This is due to the presence of defects in the frozen configurations.

Notwithstanding the eventual relaxation to a crystalline state, our systems were usually found to remain

metastable for a period of time sufficient for us to collect useful data in the critical region. Unfortunately, the freezing became unmanageable when we attempted to obtain data in the fluid-fluid coexistence region. As noted by other authors [3, 35] the coexistence curve of depletion potentials appears to be rather flat near the critical point. Thus even a modest excursion into the two phase region results in high liquid densities, which in our experience froze very rapidly.

## B. Polydisperse case

Turning now to the polydisperse case, we have obtained the critical point parameters in a manner similar to that employed in the monodisperse limit. Fig. 7 shows the comparison of our estimates for the critical point distribution  $p(\eta_b)$  for the RED potential in both the mono and polydisperse cases with  $q = 0.1$ . Clearly the distribution for the polydisperse case is substantially shifted to higher volume fractions compared to that for the monodisperse case. Owing to the slow fluctuations of  $\eta_b$ , the true average of these distributions could not be determined to high precision. However, the peak positions are rather insensitive to the fluctuations, and on the basis of critical point universality one expects that given sufficient statistics, the form of the distributions should become symmetric. One can therefore estimate  $\eta_b^{\text{crit}}$  from the average of the peak positions. The results of so doing are summarized in tab. II, from which one discovers that the principal influence of polydispersity on the critical point parameters is a significant decrease in  $\tilde{\eta}_s^{\text{crit}}$  with respect to its monodisperse value, and a significant increase in  $\eta_b^{\text{crit}}$ . For the form and degree of polydispersity we have studied, the decrease in  $\tilde{\eta}_s^{\text{crit}}$  is about 6%, while the concomitant increase in  $\eta_b^{\text{crit}}$  is about 17%.

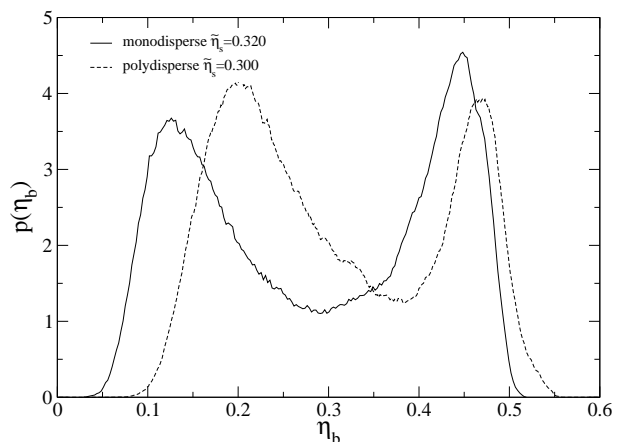


FIG. 7: Comparison of the distribution  $p(\eta_b)$  at the estimated critical parameters in the monodisperse and polydisperse systems. In both cases the size ratio  $q = 0.1$  and the system size is  $V = (6\bar{\sigma})^3$

$q$	RED potential	
	$\tilde{\eta}_s^{\text{crit}}$	$\eta_b^{\text{crit}}$
0.1	0.300(1)	0.336(15)
0.05	0.1655(5)	0.345(5)

TABLE II: Estimated critical point parameters for the model polydisperse system described in sec. IV B

The influence of polydispersity on the near critical point phase behaviour is further observable in terms of particle size fractionation effects. Specifically, when fluctuations of the instantaneous value volume fraction  $\eta_b$  exceed their average value, the distribution of particle sizes is shifted to larger diameters; and conversely for fluctuations of  $\eta_b$  to values lower than the average. The scale of the effect is shown in fig. 8 for  $q = 0.1$  at the estimated critical point parameters. The presence of such fractionation implies that the critical point need not lie at the apex of the cloud curve that marks the onset of phase separation [27]. Indeed we did observe some evidence for a weak separation of cloud and shadow curves at  $\tilde{\eta}_s = \tilde{\eta}_s^{\text{crit}}$ , although precise quantification of the effect was complicated by a noticeably increased tendency of the polydisperse system to relax to a high density state following a fluctuation to high density. The nature of this relaxation closely resembled that observed in the monodisperse case (cf. fig. 6) and indeed visualization of the arrested configurations revealed some evidence of crystalline order, albeit with a high concentration of defects. We caution, however, that these findings should not be interpreted as providing strong evidence for a freezing of the polydisperse system because it was not possible to ensure that the overall density distribution remained on the dilution line during the relaxation to the high density state.

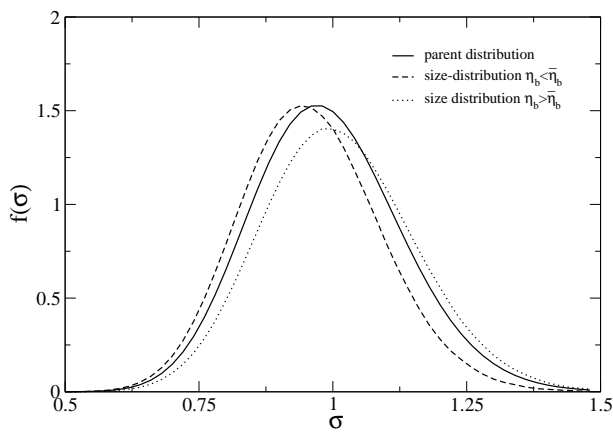


FIG. 8: The normalized distribution of particle sizes for instantaneous volume fractions  $\eta_b$  below (dashed line) and above (dotted line) the average value, close to the critical point. Also shown (solid line) is the overall Schulz “parent” distribution

### C. Percolation threshold

Percolation is a necessary, though not sufficient condition for gelation and dynamical arrest in colloidal systems. Since gelation can affect the ability of experiments to observe equilibrium phase behaviour in general, and specifically fluid-fluid phase separation, it is important to determine the location of the percolation line in the phase diagram and its relationship to the fluid-fluid critical point. Additionally, it is of interest to ask to what extent this relationship is affected by polydispersity.

In order to locate the percolation threshold, it is necessary to identify pairs of particles that are ‘bonded’ and check for spanning of clusters of such particles. However, in contrast to lattice models or fluid systems such as the adhesive hard sphere model, the definition of a ‘bond’ in systems with continuous potentials is somewhat ambiguous. We therefore adopt a criterion which derives from that used for cluster identification in spin models. Specifically, we determine the interaction energy  $u$  between all pairs of particles and assign a bond with probability  $p_{\text{bond}} = 1 - \exp(-\beta u)$ . Clusters of bonded particles are then identified using the algorithm of Hoshen and Kopelman [36]. In ref. [37] Miller and Frenkel identified the percolation threshold with those values of the model parameters for which the proportion of configurations containing a spanning cluster is 50%. However, finite-size scaling arguments [38] show that better estimates may be obtained by examining the finite-size behaviour of plots of the fraction of spanning clusters as a function of  $\eta_b$ . An example of such a plot is shown in fig. 9 for the RED potential in the monodisperse case for  $\tilde{\eta}_s = 0.28$ . Data are shown for 4 system sizes, and indicate that there is a well defined intersection point at  $\eta_b \approx 0.21$ . This intersection point provides a good measure of the percolation threshold in the thermodynamic limit [38]. By contrast, application of the 50% criterion to data for a single system size can considerably overestimate the percolation threshold.

Percolation lines were determined using this intersection method for the monodisperse and polydisperse RED potential at  $q = 0.1$ . They are shown in fig. 10 together with our estimates of the critical point parameters. One sees that in both cases the critical point lies well within the percolation regime, though much more so for the polydisperse system than for the monodisperse system.

### V. LINKING TO THE ADHESIVE HARD SPHERE MODEL

A simple yet general method for finding two potentials that are ‘equivalent’ in a corresponding states sense, is to match their second virial coefficient  $B_2$  [37, 39, 40]:

$$B_2 = -2\pi \int_0^\infty \left( e^{-\beta u(r)} - 1 \right) r^2 dr. \quad (16)$$

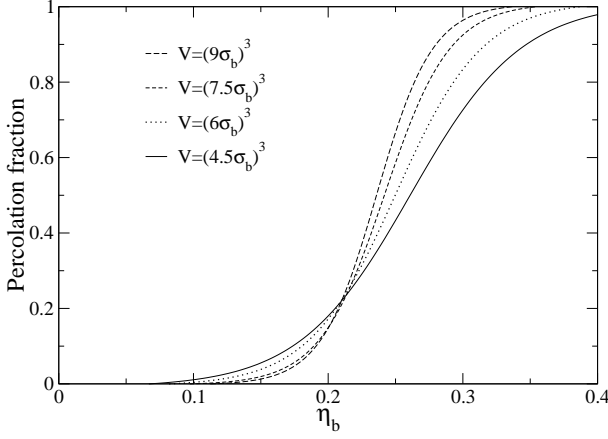


FIG. 9: Fraction of percolating configurations as a function of  $\eta_b$  for the RED potential in the monodisperse limit. The potential parameters are  $\tilde{\eta}_s = 0.28$ ,  $q = 0.1$ , and data are shown for four system sizes.

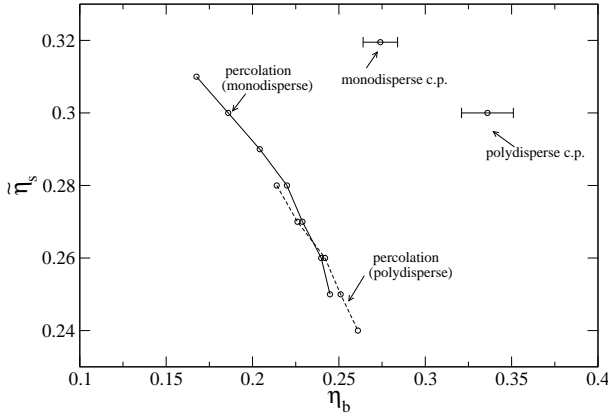


FIG. 10: Percolation line for the RED potential ( $q = 0.1$ ) for both the monodisperse and polydisperse cases, as determined by the method described in the text. Statistical errors are comparable with the symbol sizes; lines are guides to the eye. The system size in both cases was  $L = (6\sigma)^3$ . Also shown are the estimated critical point parameters (cf. sec. II B).

Here we compare the value of  $B_2$  for the RED and DRE depletion potentials in the monodisperse limit, with that of the adhesive hard sphere (AHS) model [41]. The latter comprises hard particles which experience a finite attraction only at contact, the strength of which is controlled via a ‘stickiness’ parameter  $\tau$ . The overall interaction can be written

$$e^{-\beta u(r)} = \Theta(r - \sigma) + \frac{\sigma}{12\tau} \delta(r - \sigma), \quad (17)$$

with  $r$  the separation of particle centers and  $\sigma$  the particle diameter. The second virial coefficient follows as

$$B_2^{AHS} = \frac{2\pi}{3} \sigma^3 \left( 1 - \frac{1}{4\tau} \right). \quad (18)$$

Monodisperse RED potential		
$q$	$\tilde{\eta}_s$ predicted	$\tilde{\eta}_s$ simulation
0.1	0.320	0.3195(5)
0.05	0.177	0.1765(5)
Monodisperse DRE potential		
$q$	$\tilde{\eta}_s$ predicted	$\tilde{\eta}_s$ simulation
0.1	0.256	0.255(15)
0.05	0.151	0.151(1)
Polydisperse RED potential		
$q$	$\tilde{\eta}_s$ predicted	$\tilde{\eta}_s$ simulation
0.1	0.310	0.300(1)
0.05	0.172	0.1655(5)

TABLE III: Comparison of the simulation estimates of the critical point parameters with the predictions arising by matching the second virial coefficient to that of the critical AHS model.

The AHS model exhibits a fluid-fluid phase transition, the critical point of which has been estimated to occur [42] at  $\tau_c = 0.1133(5)$ ,  $\rho_c = 0.508(10)$ . This value of  $\tau_c$  implies that for the AHS model at criticality,  $B_2^{\text{crit}} = -4.826v_0$  with  $v_0 = (4/3)\pi\sigma^3$ . It is therefore of interest to assess whether, via the matching of  $B_2$  values for the RED and DRE potentials to that of the critical AHS model, reasonable predictions can be made for the critical point parameters of the depletion potentials. To this end we have numerically evaluated  $B_2$  across a range of  $\tilde{\eta}_s$  values for each depletion potential and  $q$  value of interest. By so doing we could determine that value of  $\tilde{\eta}_s$  for which  $B_2$  matched the value  $B_2^{\text{crit}} = -4.826v_0$ . Table. III shows the resulting predictions for  $\tilde{\eta}_s^{\text{crit}}$  for two values of  $q$ , together with our simulation estimates. Clearly, in each instance, the agreement is remarkable.

One can attempt to extend the above approach to the polydisperse depletion potentials. To do so, we first obtain the contribution to the second virial coefficient for interactions between all pairs of species  $\sigma_i, \sigma_j$ . The overall coefficient for the mixture can then be approximated as a weighted average of pairs [43], where the weight factor is the probability of interaction between a pair of particles of size  $i$  and size  $j$ . In our case, this is given by the product of the corresponding values of the normalized Schulz distribution (eq.12):

$$B_2 = \int_0^\infty \int_0^\infty f(\sigma_i) f(\sigma_j) B_2(\sigma_i, \sigma_j) d\sigma_i d\sigma_j \quad (19)$$

Matching to  $B_2^{\text{crit}} = -4.826v_0$  as before, one obtains for the two  $q$  values studied, the predictions for  $\tilde{\eta}_s^{\text{crit}}$  shown in tab III. Here the agreement with the simulation estimates is less impressive than in the monodisperse case. Although the absolute value of the prediction still agrees to within about 3% with the simulation estimate, and the sign of the polydispersity-induced shift in  $\tilde{\eta}_s^{\text{crit}}$  is correctly predicted, its magnitude is underestimated by a factor of two.



The larger relative discrepancy between the predicted and measured  $\tilde{\eta}_s^{\text{crit}}$  may point to a breakdown in the presence of polydispersity of the assumed model invariance of the critical  $B_2$  value. Indeed one might expect such a failure because the value of  $B_2$  is based solely on the pair potential and takes no account of the ability of a polydisperse fluid to exploit local size segregation in order to pack more effectively than a corresponding monodisperse one. In order to address this issue directly, one would require estimates of critical point  $B_2$  values for a polydisperse version of the AHS model. To our knowledge no simulation estimates of the liquid-gas transition currently exist for a polydisperse AHS model. Indeed, the matter is complicated by the fact that there is no *unique* model for polydispersity in such a system. Very recently, however, a number of physically reasonable models for polydispersity in AHS system have been proposed by Fantoni et al [44], who investigated the corresponding phase behaviour using integral equation theory. From ref. [44], one can deduce that the presence of polydispersity significantly *decreases* the magnitude of  $B_2$  at the critical point compared to the monodisperse limit. This trend in  $B_2$  is of the correct sign and overall magnitude to push the predictions for  $\tilde{\eta}_s^{\text{crit}}$  for our depletion potentials closer to the simulation estimates. Unfortunately since no data were reported for exactly the same degree of polydispersity ( $\delta = 14\%$ ) studied in the present work, no direct comparison of  $B_2$  values is possible.

In an attempt to throw additional light (albeit indirectly) on the discrepancy between the measured and predicted critical point parameters, we have studied the effect of introducing polydispersity on the critical point  $B_2$  value for the Lennard-Jones fluid, which is a computationally more tractable system than the AHS model [45]. The corresponding potential is

$$u_{ij} = \epsilon_{ij} \left[ \left( \frac{\sigma_{ij}}{r_{ij}} \right)^{12} - \left( \frac{\sigma_{ij}}{r_{ij}} \right)^6 \right] \quad (20)$$

with  $\epsilon_{ij} = \sigma_i \sigma_j \epsilon$ ,  $\sigma_{ij} = (\sigma_i + \sigma_j)/2$  and  $r_{ij} = |\mathbf{r}_i - \mathbf{r}_j|$ . The potential was cutoff for  $r_{ij} > 2.5\sigma_{ij}$  and no tail corrections were applied. For the monodisperse limit, the critical temperature occurs at  $T_c = 1.1876(3)$  [32] and one finds  $B_2 = -6.621v_0$ , which lies within the range of ‘typical’ critical point  $B_2$  values found in surveys of a wide range of model potentials [39, 40]. If, on the other hand,  $\sigma$  is distributed according to a Schulz form (eq.12) with  $z = 50$ , as used elsewhere in this work, simulations yield a critical temperature of  $T_c = 1.384(1)$ , for which (using eq. 19), one finds  $B_2 = -5.759v_0$ , which is significantly smaller in magnitude than the monodisperse value.

If one now makes the (not unreasonable) assumption that given the same form and degree of polydispersity, a comparable fractional change of  $B_2$  will ensue in other interaction potentials, one can estimate the expected critical point value of  $B_2$  for the polydisperse AHS model

(and hence also the polydisperse depletion potentials), as  $B_2 = -4.826 \times 5.759/6.621 \approx -4.2v_0$ . The resulting predictions for the critical reservoir volume fraction of the small particles are  $\tilde{\eta}_s^{\text{crit}} = 0.304$ , for  $q = 0.1$ , and  $\tilde{\eta}_s^{\text{crit}} = 0.169$  for  $q = 0.05$ , both of which agree within error with our simulation results. Of course in view of our assumptions, this accord may be fortuitous, but it is nevertheless suggestive that a more detailed assessment of the effect of polydispersity on critical point  $B_2$  values in other systems (specifically the AHS model) would be a worthwhile avenue for further study.

## VI. CONCLUSIONS AND DISCUSSION

To summarize, we have determined the effect of introducing polydispersity on the fluid-fluid critical point parameters of a model depletion potential for highly asymmetric additive hard sphere mixtures. For the particular realization of the polydispersity considered, the critical point is found to shift (with respect to the monodisperse limit) to smaller values of the reservoir volume fraction of the small particles  $\tilde{\eta}_s$  and to larger values of the volume fraction of the large particle  $\tilde{\eta}_b$ . It seems reasonable to assume that the direction of the shifts should be a general trend, common to other functional forms and degree of polydispersity. Indeed the same trend has also recently been observed in a study of colloidal polydispersity in the AO model [11].

Beyond this, our results show that inclusion of polydispersity pushes the whole fluid-fluid binodal deeper into the percolating regime. Since colloidal fluids are known to form a gel [46, 47] for sufficiently high  $\tilde{\eta}_s$ , it would seem that the presence of polydispersity increases the likelihood that direct observations of fluid-fluid phase coexistence is complicated by dynamical arrest.

Additionally we demonstrated that excellent predictions for the value of  $\tilde{\eta}_s^{\text{crit}}$  follow from matching the second virial coefficient  $B_2$  of depletion potentials to the critical  $B_2$  value of the adhesive hard sphere model. The quantitative accuracy of the predictions is undoubtedly due in large part to the very short ranged nature of the depletion potentials; similar studies comparing critical point  $B_2$  values for a range of other potentials [39, 40] did not find such a high degree of accuracy. Nevertheless our observation should prove generally useful in reducing the effort required to locate criticality in depletion potentials. It is intriguing however, that the accuracy of the predictions was reduced on incorporating polydispersity, suggesting that (perhaps due to changes in packing ability due to local size segregation effects), the inclusion of polydispersity in a model does not leave  $B_2$  invariant at the critical point. Comparisons of the critical  $B_2$  value for a monodisperse and polydisperse LJ fluid confirmed a significant difference in this regard. Moreover, the magnitude of the effect was sufficient to account for the discrepancy in the observed and predicted  $\tilde{\eta}_s^{\text{crit}}$  for the polydisperse depletion potential. Clearly, however,

further work is called for in order to elucidate this matter more fully.

Obviously knowledge of the shift in the critical point parameters is in itself insufficient to determine whether polydispersity renders the fluid-fluid transition stable with respect to fluid-solid coexistence. Although we did observe a spontaneous relaxation of the near critical polydisperse system to a high density state showing some crystalline order, this finding should be treated with caution because the system departs from the dilution line during the formation of the new state. It would thus be interesting in future work to try to study explicitly the effects of polydispersity on the freezing transition. As well as providing assessment of the overall stability of the fluid-fluid critical point, freezing in polydisperse fluids is a matter of considerable interest in its own right. Indeed recent theoretical calculations for the AO model indicate an increasing richness of fluid-solid and solid-solid phase behaviour as the degree of polydispersity is increased [11]. To tackle this computationally, however, is a considerable challenge, but one which might be met by extending to polydisperse system novel computational methods which have hitherto only be deployed in the monodisperse con-

text [48, 49].

Finally, we remark that while the present work has considered solely the case of polydispersity of the large particles, the converse situation of small particles polydispersity is clearly of interest and practical relevance too. While there have been several theoretical studies which have considered this scenario (see eg. refs. [17, 50]), we know of no simulation studies to date. An extension of the methods utilised here to address this case would doubtless be a worthwhile endeavor—one which we hope to undertake in future work.

### Acknowledgments

The authors are grateful to R. Evans and A. Louis for helpful discussions and advice, and to M. Dijkstra for supplying data from ref. [3]. This work was supported by EPSRC, grant number GR/S59208/01. JL acknowledge support from Spanish Ministerio de Educacion, Cultura y Deporte.

- 
- [1] For a general overview of colloidal interactions, see L. Belloni, *J. Phys.: Condens. Matter*, **12**, 549 (2000).
  - [2] T. Biben and J.P. Hansen, *Phys. Rev. Lett.* **66**, 2215 (1991).
  - [3] M. Dijkstra, R. van Roij, R. Evans, *Phys. Rev. Lett.*, **81**, 2268 (1998); M. Dijkstra, R. van Roij, and R. Evans, *Phys. Rev. Lett.*, **82**, 117 (1999); M. Dijkstra, R. van Roij, and R. Evans, *Phys. Rev. E*, **59**, 5744 (1999).
  - [4] N.G. Almaraz and E. Enciso, *Phys. Rev.* **E59**, 4426 (1999).
  - [5] W.C.K. Poon, *J. Phys.: Condens. Matter*, **14**, 859 (2002).
  - [6] A. Buhot and W. Krauth, *Phys. Rev. Lett.* **80**, 3787 (1998).
  - [7] J. Liu and E. Luijten, *Phys. Rev.* **E71**, 066701 (2005).
  - [8] R. Roth, R. Evans, and S. Dietrich, *Phys. Rev. E*, **62**, 5360 (2000).
  - [9] L. Bellier-Castella, H. Xu and M. Baus, *J. Chem. Phys.* **113**, 8337 (2000).
  - [10] N.B. Wilding, M. Fasolo and P. Sollich, *J. Chem. Phys.* **121**, 6887 (2004).
  - [11] M. Fasolo and P. Sollich, *J. Chem. Phys.* **122**, 074904 (2005).
  - [12] D.A. Kofke and P.G. Bolhuis, *Phys. Rev. E* **54**, 634 (1996); *ibid* **59**, 618 (1999).
  - [13] P.B. Warren, *Europhys. Lett.*, **46**, 295 (1999).
  - [14] P. Sollich and M.E. Cates, *Phys. Rev. Lett.* **80** 1365 (1998); P.B. Warren, *Phys. Rev. Lett.* **80** 1369 (1998);
  - [15] T. Boublík, *J. Chem. Phys.* **53**, 471 (1970); G.A. Mansoori, N.F. Carnahan, K.E. Starling, T.W. Leland, *J. Chem. Phys.* **54**, 1523 (1971).
  - [16] Y. Mao, *J. Phys. II*, **5**, 1761 (1995).
  - [17] D. Goulding, and J.-P. Hansen, *Mol. Phys.*, **99**, 865 (2001).
  - [18] D. Frydel and S. A. Rice, *Phys. Rev.* **E71**, 041403 (2005).
  - [19] S. Asakura and F. Oosawa, *J. Chem. Phys.* **22** 1255 (1954).
  - [20] M. Dijkstra, J.M. Brader and R. Evans, *J. Phys. Condens. Matter* **11**, 10079 (1999).
  - [21] R.L.C. Vink, and J. Horbach, *J. Phys.: Condens. Matter*, **16**, 3807 (2004); R.L.C. Vink and M. Schmidt, *Phys. Rev. E* **71**, 051406 (2005).
  - [22] B. Götzelmann, R. Evans, and S. Dietrich, *Phys. Rev. E*, **57**, 6785 (1998).
  - [23] B. Götzelmann, R. Roth, S. Dietrich, M. Dijkstra, and R. Evans, *Europhys. Lett.*, **47**, 398 (1999).
  - [24] B.V. Derjaguin, *Kolloid-Z.* **69**, 155 (1934).
  - [25] W.B. Russel, D.A. Saville, and W.R. Schowalter, *Colloidal Dispersions*, Cambridge University Press (1989)
  - [26] G.V. Schulz, *Z. Physik. Chem.* **B43**, 25 (1939); B.H. Zimm, *J. Chem. Phys.* **16**, 1099 (1948).
  - [27] P. Sollich, *J. Phys. Condens. Matter*, **14**, R79 (2002).
  - [28] N.B. Wilding and P. Sollich, *Europhys. Lett.* **67** 219 (2004).
  - [29] N.B. Wilding, *J. Chem. Phys.* **119**, 12163 (2003).
  - [30] N.B. Wilding and P. Sollich, *J. Chem. Phys.* **116**, 7116 (2002).
  - [31] A.M. Ferrenberg and R.H. Swendsen, *Phys. Rev. Lett.* **61**, 2635 (1988); *ibid* **63**, 1195 (1989).
  - [32] N.B. Wilding, *Phys. Rev.* **E52** 602 (1995); N.B. Wilding and A.D. Bruce, *J. Phys. Condens. Matter*, **4**, 3087 (1992).
  - [33] Ph. Germain, J.G. Malherbe and S. Amokrane, *Phys. Rev. E* **70**, 041409 (2004).
  - [34] J. Clément-Cottuz, S. Amokrane, and C. Regnaut, *Phys. Rev. E* **61**, 1692 (2000).
  - [35] F. Lo Verso, D. Pini, and L. Reatto, *J. Phys.: Condens. Matter*, **17**, 771 (2005).
  - [36] J. Hoshen, and R. Kopelman, *Phys. Rev. B*, **14**, 3438

- (1976).
- [37] M. A. Miller, and D. Frenkel, Phys. Rev. Lett., **90**, 135702-1 (2003).
  - [38] K. Binder and D.W. Heermann, *Monte Carlo Simulation in Statistical Physics*, Springer, Berlin (1992).
  - [39] G.A. Vliegenthart and H.N.W. Lekkerkerker, J. Chem. Phys. **112**, 5364 (2000).
  - [40] M.G. Noro, and D. Frenkel, J. Chem. Phys **113**, 2941 (2000).
  - [41] R.J. Baxter, J. Chem. Phys. **49**, 2270 (1968).
  - [42] M.A. Miller, and D. Frenkel, J. Chem. Phys., **121**, 535 (2004).
  - [43] K.R. Hall, G. A. Iglesias-Silva, and G. A. Mansoori, Fluid Phase Equilibria, **91**, 67 (1993)
  - [44] R. Fantoni, D. Gazzillo and A. Giacometti, J. Chem. Phys. **122**, 034901 (2005).
  - [45] M.A. Miller, and D. Frenkel, J. Phys.: Condens. Matter, **16**, S4901 (2004).
  - [46] J. Bergenholtz, M. Fuchs, and Th. Voigtmann, J. Phys.: Condens. Matter, **12**, 6575 (2000).
  - [47] M.E. Cates, M. Fuchs, K. Kroy, W.C.K. Poon, and A.M. Puertas, J. Phys.: Condens. Matter, **16**, 4861 (2004).
  - [48] N.B. Wilding and A.D. Bruce, Phys. Rev. Lett. **85**, 5138 (2000).
  - [49] G.C. McNeil-Watson and N.B. Wilding (unpublished)
  - [50] M. Fasolo and P. Sollich, J. Phys. Condens Matter **17**, 797 (2005).